to attribute the rapid optical/IR brightness increase of this source to a sharp transition from relatively slow to exceedingly rapid accretion[13,15,16]. The contemporaneous X-ray burst therefore is also best explained as ultimately due to accretion. The inferred post-outburst X-ray temperature was far too high for the X-rays to be generated by shocks resulting from accretion onto a low-mass, pre-MS star, however[12]. Instead, the burst of X-rays was most probably generated via star–disk magnetic reconnection events that occurred in conjunction with such mass infall. This process may also launch new, collimated outflows or jets. Indeed, before its recent eruption, the pre-MS star in L1630 had been identified as the exciting source of a chain of extended emission nebulosity that appears to terminate at a shock-excited Herbig–Haro object (HH 23)[26]. The presence of these structures suggests that the present optical/IR/X-ray outburst from this object may be merely the latest of a series of such events.

If FU Ori stars are indeed among the most rapidly accreting pre-MS stars[16], and X-rays from pre-MS stars can be ascribed in part to accretion, then one would naively expect all FU Ori stars to be luminous pre-MS X-ray sources. It is noteworthy, then, that before the observations reported here only two FU Ori candidates, Z CMa and L1551 IRS5, had been detected in X-rays; furthermore, both exhibit very low L_X/L_{bol} ratios[27,28] of $\sim 10^{-6}$, compared with $L_X/L_{bol} \approx 10^{-3}$ for the erupting young star in L1630 (as estimated near the peak of its outburst). This suggests that the very large accretion rates during the steady-state phase following an FU Ori outburst eventually push the star–disk boundary sufficiently close to the stellar photosphere that the accretion becomes non-magnetospheric[29], thereby effectively 'quenching' X-ray emission from such objects long before the rapid accretion phase itself subsides. The precipitous drop in the X-ray flux and spectral hardness of the erupting L1630 pre-MS star, post-outburst, may signal the onset of this quenching phase, or it may indicate that the abrupt change in the nature of the star–disk interactions has triggered a phase of strong variability in both X-ray luminosity and temperature. □

Received 19 April; accepted 14 June 2004; doi:10.1038/nature02747.

1. Feigelson, E. D. & Montmerle, T. High-energy processes in young stellar objects. *Annu. Rev. Astron. Astrophys.* **37,** 363–408 (1999).
2. Preibisch, T., Neuhaeuser, R. & Alcala, J. M. A giant X-ray flare on the young star P1724. *Astron. Astrophys.* **304,** L13–L16 (1995).
3. Koyama, K., Hamaguchi, K., Ueno, S., Kobayashi, N. & Feigelson, E. D. Discovery of hard X-rays from a cluster of protostars. *Publ. Astron. Soc. Jpn* **48,** L87–L92 (1996).
4. Grosso, N. *et al.* An X-ray superflare from an infrared protostar. *Nature* **387,** 56–58 (1997).
5. Ozawa, H., Nagase, F., Ueda, Y., Dotani, T. & Ishida, M. Detection of hard X-rays from a class I protostar in the HH 24-26 region in the Orion molecular cloud. *Astrophys. J.* **523,** L81–L84 (1999).
6. Imanishi, K., Koyama, K. & Tsuboi, Y. Chandra observation of the rho Ophiuchi cloud. *Astrophys. J.* **557,** 747–760 (2001).
7. Feigelson, E. D., Garmire, G. P. & Pravdo, S. Magnetic flaring in the pre-main-sequence Sun and implications for the early Solar System. *Astrophys. J.* **572,** 335–349 (2002).
8. Kastner, J. H. *et al.* The coronal X-ray spectrum of the multiple weak-lined T Tauri star system HD 98800. *Astrophys. J.* **605,** L49–L52 (2004).
9. Stassun, K. G., Ardila, D. R., Barsony, M., Basri, G. & Mathieu, R. D. X-ray properties of pre-main-sequence stars in the Orion nebula cluster with known rotation periods. *Astron. J.* **127,** 3537–3552 (2004).
10. Shu, F. H., Shang, H., Glassgold, A. E. & Lee, T. X-rays and fluctuating X-winds from protostars. *Science* **277,** 1475–1479 (1997).
11. Kastner, J. H., Huenemoerder, D. P., Schulz, N. S., Canizares, C. R. & Weintraub, D. A. Evidence for accretion: High-resolution X-ray spectroscopy of the classical T Tauri star TW Hydrae. *Astrophys. J.* **567,** 434–440 (2002).
12. Stelzer, B. & Schmitt, J. H. M. M. X-ray emission from a metal depleted accretion shock onto the classical T Tauri star TW Hya. *Astron. Astrophys.* **418,** 687–697 (2004).
13. Briceno, C. *et al.* McNeil's nebula in Orion: The outburst history. *Astrophys. J.* **606,** L123–L126 (2004).
14. McNeil, J. W. *IAU Circ. No.* 8284 (2004)
15. Reipurth, B. & Aspin, C. IRAS 05436-0007 and the emergence of McNeil's nebula. *Astrophys. J.* **606,** L119–L122 (2004).
16. Hartmann, L. & Kenyon, S. J. The FU Orionis phenomenon. *Annu. Rev. Astron. Astrophys.* **34,** 207–240 (1996).
17. Herbig, G. H. Eruptive phenomena in early stellar evolution. *Astrophys. J.* **217,** 693–715 (1977).
18. Herbig, G. H., Aspin, C., Gilmore, A. C., Imhoff, C. L. & Jones, A. F. The 1993-1994 activity of EX Lupi. *Publ. Astron. Soc. Pacif.* **113,** 1547–1553 (2001).
19. Montmerle, T., Grosso, N., Tsuboi, Y. & Koyama, K. Rotation and X-ray emission from protostars. *Astrophys. J.* **532,** 1097–1110 (2000).
20. Hayashi, M., Shibata, K. & Matsumoto, R. X-ray flares and mass outflows driven by magnetic interaction between a protostar and its surrounding disk. *Astrophys. J.* **468,** L37–L40 (1996).
21. Goodson, A. P., Winglee, R. M. & Boehm, K.-H. Time-dependent accretion by magnetic young stellar objects as a launching mechanism for stellar jets. *Astrophys. J.* **489,** 199–209 (1997).
22. Simon, T., Andrews, S. M., Rayner, J. T. & Drake, S. A. X-ray and infrared observations of embedded young stars in L1630. *Astrophys. J.* (in the press); preprint at ⟨http://arXiv.org/astro-ph/0404260⟩ (2004).
23. Anthony-Twarog, B. J. The H-beta distance scale for B stars—The Orion association. *Astron. J.* **87,** 1213–1222 (1982).
24. Feigelson, E. D. *et al.* X-ray-emitting young stars in the Orion nebula. *Astrophys. J.* **574,** 258–292 (2002).
25. Ábrahám, P. *et al.* The infrared properties of the new outburst star IRAS 05436-0007 in quiescent phase. *Astron. Astrophys.* **419,** L39–L42 (2004).
26. Eisloffel, J. & Mundt, R. Parsec-scale jets from young stars. *Astron. J.* **114,** 280–287 (1997).
27. Zinnecker, H. & Preibisch, Th. X-ray emission from Herbig Ae/Be stars: A ROSAT survey. *Astron. Astrophys.* **292,** 152–164 (1994).
28. Favata, F., Fridlund, C. V. M., Micela, G., Sciortino, S. & Kaas, A. A. Discovery of X-ray emission from the protostellar jet L1551 IRS5 (HH 154). *Astron. Astrophys.* **386,** 204–210 (2002).
29. Hartmann, L. *Accretion Processes in Star Formation* (Cambridge Univ. Press, Cambridge, 1998).
30. Kaastra, J. S., Mewe, R. & Nieuwenhuijzen, H. in *UV and X-ray Spectroscopy of Astrophysical and Laboratory Plasmas* (eds Yamashita, K. & Watanabe, T.) 411 (Universal Academy Press, Tokyo, 1996).

Acknowledgements CXO observations of the erupting object in L1630 acquired in March 2004 were obtained under allocations of CXC Director's Discretionary Time. XSPEC software is maintained by NASA's High Energy Astrophysics Science Archive Research Center. The archival optical image in Fig. 2 was obtained with ESO's VLT at the Paranal Observatories under program ID 272.C-5045. We thank B. L. Gary for communicating results of I-band monitoring of the source.

Competing interests statement The authors declare that they have no competing financial interests.

Correspondence and requests for materials should be addressed to J.H.K. (jhk@cis.rit.edu).

Single-shot read-out of an individual electron spin in a quantum dot

J. M. Elzerman, R. Hanson, L. H. Willems van Beveren, B. Witkamp, L. M. K. Vandersypen & L. P. Kouwenhoven

Kavli Institute of Nanoscience Delft and ERATO Mesoscopic Correlation Project, Delft University of Technology, PO Box 5046, 2600 GA Delft, The Netherlands

Spin is a fundamental property of all elementary particles. Classically it can be viewed as a tiny magnetic moment, but a measurement of an electron spin along the direction of an external magnetic field can have only two outcomes[1]: parallel or anti-parallel to the field. This discreteness reflects the quantum mechanical nature of spin. Ensembles of many spins have found diverse applications ranging from magnetic resonance imaging[2] to magneto-electronic devices[3], while individual spins are considered as carriers for quantum information. Read-out of single spin states has been achieved using optical techniques[4], and is within reach of magnetic resonance force microscopy[5]. However, electrical read-out of single spins[6–13] has so far remained elusive. Here we demonstrate electrical single-shot measurement of the state of an individual electron spin in a semiconductor quantum dot[14]. We use spin-to-charge conversion of a single electron confined in the dot, and detect the single-electron charge using a quantum point contact; the spin measurement visibility is ~65%. Furthermore, we observe very long single-spin energy relaxation times (up to ~0.85 ms at a magnetic field of 8 T), which are encouraging for the use of electron spins as carriers of quantum information.

In quantum dot devices, single electron charges are easily measured. Spin states in quantum dots, however, have only been studied by measuring the average signal from a large ensemble of electron spins[15–20]. In contrast, the experiment presented here aims at a single-shot measurement of the spin orientation (parallel or antiparallel to the field, denoted as spin-↑ and spin-↓, respectively) of

a particular electron; only one copy of the electron is available, so no averaging is possible. The spin measurement relies on spin-to-charge conversion[18,19] followed by charge measurement in a single-shot mode[21,22]. Figure 1a schematically shows a single electron spin confined in a quantum dot (circle). A magnetic field is applied to split the spin-↑ and spin-↓ states by the Zeeman energy. The dot potential is then tuned such that if the electron has spin-↓ it will leave, whereas it will stay on the dot if it has spin-↑. The spin state has now been correlated with the charge state, and measurement of the charge on the dot will reveal the original spin state.

This concept is implemented using a structure[23] (Fig. 1b) consisting of a quantum dot in close proximity to a quantum point contact (QPC). The quantum dot is used as a box to trap a single electron, and the QPC is operated as a charge detector in order to determine whether the dot contains an electron or not. The quantum dot is formed in the two-dimensional electron gas (2DEG) of a GaAs/AlGaAs heterostructure by applying negative voltages to the metal surface gates M, R and T (Fig. 1b). This depletes the 2DEG below the gates and creates a potential minimum in the centre, that is, the dot (indicated by a dotted white circle). We tune the gate voltages such that the dot contains either zero or one electron (which we can control by the voltage applied to gate P). Furthermore, we make the tunnel barrier between gates R and T sufficiently opaque that the dot is completely isolated from the drain contact on the right. The barrier to the reservoir on the left is set[24] to a tunnel rate $\Gamma \approx (0.05\,\mathrm{ms})^{-1}$. When an electron tunnels on or off the dot, it changes the electrostatic potential in its vicinity, including the region of the nearby QPC (defined by R and Q). The QPC is set in the tunnelling regime, so that the current, I_{QPC}, is very sensitive to electrostatic changes[25]. Recording changes in I_{QPC} thus permits us to measure on a timescale of about 8 μs whether an electron resides on the dot or not (L.M.K.V. *et al.*, manuscript in preparation). In this way the QPC is used as a charge detector with a resolution much better than a single electron charge and a measurement timescale almost ten times shorter than $1/\Gamma$.

The device is placed inside a dilution refrigerator, and is subjected to a magnetic field of 10 T (unless noted otherwise) in the plane of the 2DEG. The measured Zeeman splitting in the dot[19], $\Delta E_Z \approx 200\,\mu\mathrm{eV}$, is larger than the thermal energy (25 μeV) but smaller than the orbital energy level spacing (1.1 meV) and the charging energy (2.5 meV).

To test our single-spin measurement technique, we use an experimental procedure, inspired by earlier time-averaged measurements[18,19], that is based on three stages: (1) empty the dot, (2) inject one electron with unknown spin, and (3) measure its spin state. The different stages are controlled by voltage pulses on gate P (Fig. 2a), which shift the dot's energy levels (Fig. 2c). Before the pulse the dot is empty, as both the spin-↑ and spin-↓ levels are above the Fermi energy of the reservoir, E_F. Then a voltage pulse pulls both levels below E_F. It is now energetically allowed for an electron to tunnel onto the dot, which will happen after a typical time $\sim\Gamma^{-1}$. The particular electron can have spin-↑ or spin-↓, shown in the lower and upper diagram respectively (the tunnel rate for spin-↑ electrons is

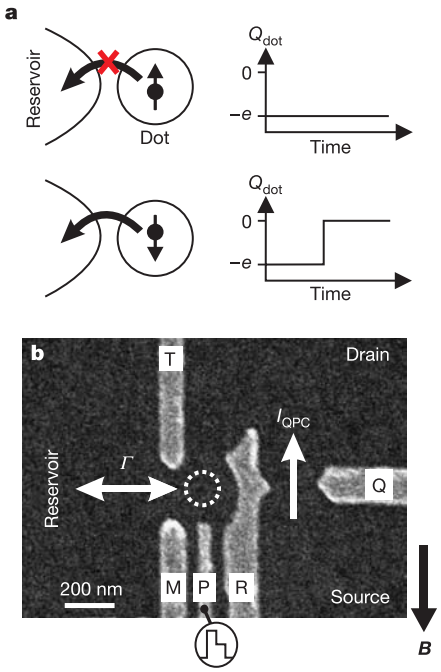

Figure 1 Spin-to-charge conversion in a quantum dot coupled to a quantum point contact. **a**, Principle of spin-to-charge conversion. The charge on the quantum dot, Q_{dot}, remains constant if the electron spin is ↑, whereas a spin-↓ electron can escape, thereby changing Q_{dot}. **b**, Scanning electron micrograph of a device like the one used in the measurements, showing the metallic gates (T, M, P, R, Q) on the surface of a GaAs/AlGaAs heterostructure containing a two-dimensional electron gas (2DEG) 90 nm below the surface. The electron density is $2.9 \times 10^{15}\,\mathrm{m}^{-2}$. (Only the gates used in the present experiment are shown, the complete device[23] is described in Supplementary Fig. S1.) By measuring the current through the QPC channel, I_{QPC}, we can detect changes in Q_{dot} that result from electrons tunnelling between the dot and the reservoir (with a tunnel rate Γ). A magnetic field, B, is applied in the plane of the 2DEG.

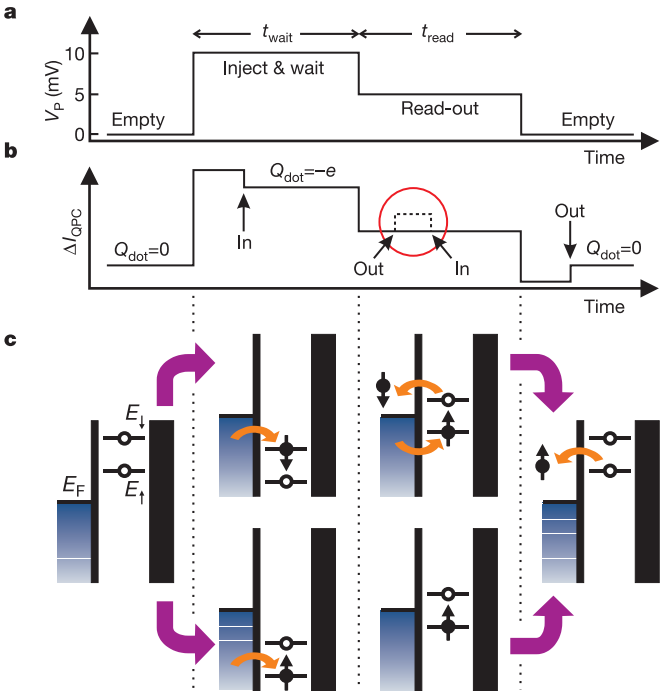

Figure 2 Two-level pulse technique used to inject a single electron and measure its spin orientation. **a**, Shape of the voltage pulse applied to gate P. The pulse level is 10 mV during t_{wait} and 5 mV during t_{read} (which is 0.5 ms for all measurements). **b**, Schematic QPC pulse-response if the injected electron has spin-↑ (solid line) or spin-↓ (dotted line; the difference with the solid line is only seen during the read-out stage). Arrows indicate the moment an electron tunnels into or out of the quantum dot. **c**, Schematic energy diagrams for spin-↑ ($E_↑$) and spin-↓ ($E_↓$) during the different stages of the pulse. Black vertical lines indicate the tunnel barriers. The tunnel rate between the dot and the QPC drain on the right is set to zero. The rate between the dot and the reservoir on the left is tuned to a specific value, Γ. If the spin is ↑ at the start of the read-out stage, no change in the charge on the dot occurs during t_{read}. In contrast, if the spin is ↓, the electron can escape and be replaced by a spin-↑ electron. This charge transition is detected in the QPC current (dotted line inside red circle in **b**).

expected to be larger than that for spin-↓ electrons[26], that is, $\Gamma_\uparrow > \Gamma_\downarrow$, but we do not assume this a priori.) During this stage of the pulse, lasting t_{wait}, the electron is trapped on the dot and Coulomb blockade prevents addition of a second electron. After t_{wait} the pulse is reduced, in order to position the energy levels in the read-out configuration. If the electron spin is ↑, its energy level is below E_F, so the electron remains on the dot. If the spin is ↓, its energy level is above E_F, so the electron tunnels to the reservoir after a typical time $\sim\Gamma_\downarrow^{-1}$. Now Coulomb blockade is lifted and an electron with spin-↑ can tunnel onto the dot. This occurs on a timescale $\sim\Gamma_\uparrow^{-1}$ (with $\Gamma = \Gamma_\uparrow + \Gamma_\downarrow$). After t_{read}, the pulse ends and the dot is emptied again.

The expected QPC response, ΔI_{QPC}, to such a two-level pulse is the sum of two contributions (Fig. 2b). First, owing to a capacitive coupling between pulse gate and QPC, ΔI_{QPC} will change proportionally to the pulse amplitude. Thus, ΔI_{QPC} versus time resembles a two-level pulse. Second, ΔI_{QPC} tracks the charge on the dot, that is, it goes up whenever an electron tunnels off the dot, and it goes down by the same amount when an electron tunnels onto the dot. Therefore, if the dot contains a spin-↓ electron at the start of the read-out stage, ΔI_{QPC} should go up and then down again. We thus expect a characteristic step in ΔI_{QPC} during t_{read} for spin-↓ (dotted trace inside red circle). In contrast, ΔI_{QPC} should be flat during t_{read} for a spin-↑ electron. Measuring whether a step is present or absent during the read-out stage constitutes our spin measurement.

Figure 3a shows typical experimental traces of the pulse-response recorded after proper tuning of the d.c. gate voltages (see Supplementary Fig. S2). We emphasize that each trace involves injecting

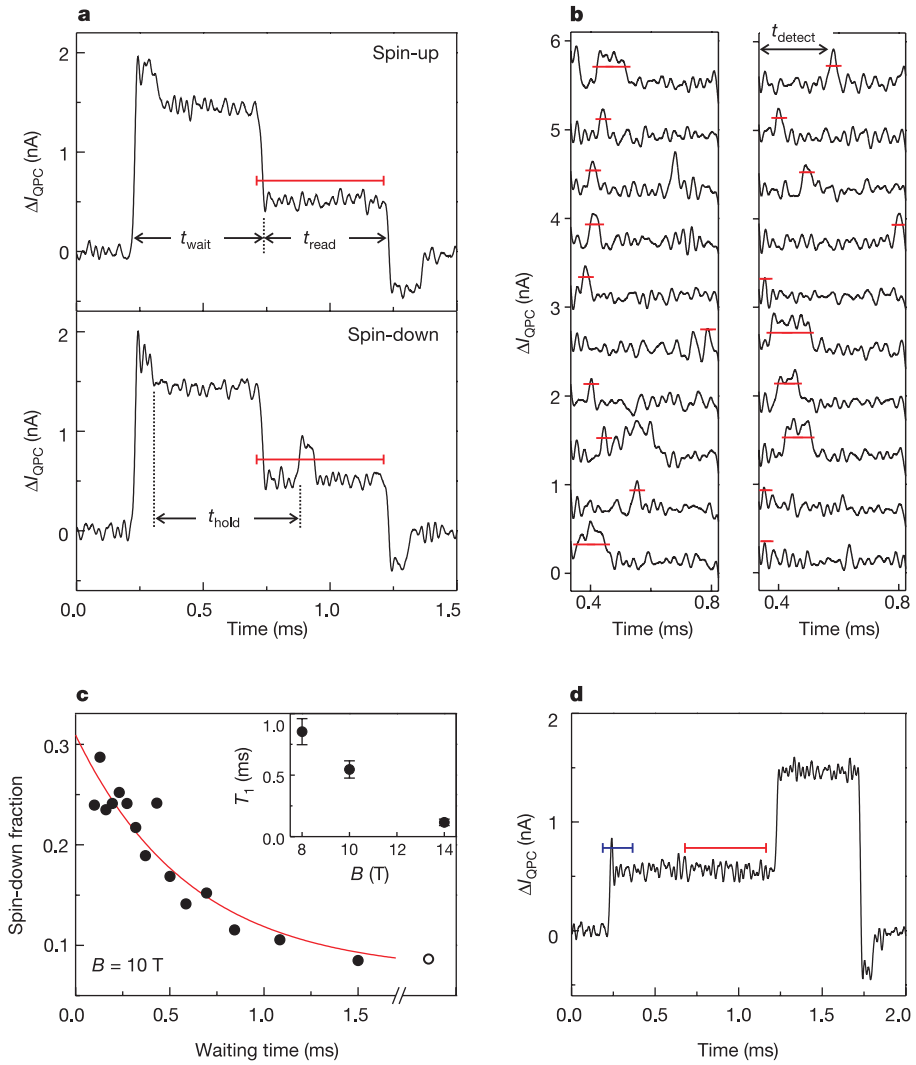

Figure 3 Single-shot read-out of one electron spin. **a**, Typical time-resolved measurements of the QPC current in response to a two-level pulse. In the top panel, an electron is injected during t_{wait} and is declared 'spin-up' during t_{read}. In the lower panel, the injected electron is declared 'spin-down' by the characteristic step which crosses the threshold (red line) during t_{read}. The total time the electron spends in the dot is defined as t_{hold}. **b**, Randomly chosen examples of traces for which the electron is declared 'spin-down' (here for the case of $t_{wait} = 0.1$ ms). Only the read-out segment is shown, and traces are offset for clarity. The actual time when ΔI_{QPC} first crosses the threshold (red line), t_{detect}, is recorded to make the histogram in Fig. 4a. **c**, Fraction of traces counted as spin-down versus waiting time, t_{wait}, out of a total of 625 traces taken for each waiting time. Rightmost point (open dot): spin-down fraction using modified pulse shape (**d**). Red solid line: exponential fit to the data. Inset: T_1 versus B (see Supplementary Fig. S4). Error bars represent the root mean square of the standard errors obtained from exponential fits to three separate data sets. **d**, Typical QPC signal for a 'reversed' pulse, which has the same amplitudes as in Fig. 2a, but with the order of the two stages reversed. In this case injection takes place with $E_\uparrow$ below and $E_\downarrow$ above E_F (see Fig. 2c, third column), so that only a spin-↑ electron can be injected. By recording the fraction of traces in which the current nevertheless crosses the threshold of duration t_{read} (red line), an independent measure of the 'dark count' probability is obtained (see text). This fraction is plotted as the open dot in **c**. It is used in the exponential fit with an associated value of $t_{wait} = 10$ ms (that is, much longer than the spin relaxation time). The blue threshold is used in Fig. 4b.

one particular electron onto the dot and subsequently measuring its spin state. Each trace is therefore a single-shot measurement. The traces that we obtain fall into two different classes; most traces qualitatively resemble the one in the top panel of Fig. 3a, some resemble the one in the bottom panel (and sometimes, no electron was injected during the injection stage; such cases were detected, see Supplementary Fig. S3, and ignored). These two typical traces indeed correspond to the signals expected for a spin-↑ and a spin-↓ electron (Fig. 2b), a strong indication that the electron in the top panel of Fig. 3a was spin-↑ and in the bottom panel spin-↓. The distinct signature of the two types of responses in ΔI_{QPC} permits a simple criterion for identifying the spin: if ΔI_{QPC} crosses the threshold value (red line in Fig. 3a and chosen as explained below), we declare the electron 'spin-down'; otherwise we declare it 'spin-up'. Figure 3b shows the read-out section of 20 more 'spin-down' traces, to illustrate the stochastic nature of the tunnel events.

The random injection of spin-↑ and spin-↓ electrons prevents us from checking the outcome of any individual measurement. Therefore, in order to further establish the correspondence between the actual spin state and the outcome of our spin measurement, we change the probability of having a spin-↓ at the beginning of the read-out stage, and compare this with the fraction of traces in which the electron is declared 'spin-down'. As t_{wait} is increased, the time between injection and read-out, t_{hold}, will vary accordingly ($t_{hold} \approx t_{wait}$). The probability for the spin to be ↓ at the start of t_{read} will thus decay exponentially to zero, since electrons in the excited spin state will relax to the ground state ($k_BT \ll \Delta E_Z$). For a set of 15 values of t_{wait} we take 625 traces for each t_{wait}, and count the fraction of traces in which the electron is declared 'spin-down' (Fig. 3c). The fact that the expected exponential decay is clearly reflected in the data confirms the validity of the spin read-out procedure.

We extract a single-spin energy relaxation time, T_1, from fitting the data points in Fig. 3c (and two other similar measurements) to $\alpha + C\exp(-t_{wait}/T_1)$, and obtain an average value of $T_1 \approx (0.55 \pm 0.07)$ ms at 10 T. This is an order of magnitude longer than the lower bound on T_1 established earlier[19], and clearly longer than the time needed for the spin measurement (of order $1/\Gamma_\downarrow \approx 0.11$ ms). Similar experiments at 8 T give $T_1 \approx (0.85 \pm 0.11)$ ms, and at 14 T we find $T_1 \approx (0.12 \pm 0.03)$ ms (Supplementary Fig. S4). More experiments are needed in order to test the theoretical prediction that relaxation at high magnetic fields is dominated by spin–orbit interactions[27–29], with smaller contributions resulting from hyperfine interactions with the nuclear spins[27,30] (co-tunnelling is insignificant given the very small tunnel rates). For both mechanisms, T_1 is expected to decrease rapidly with magnetic field[27–30], in part because the energy from the spin-flip process must be absorbed by the phonon bath, which has a higher density of states at higher energies. We note that the obtained values for T_1 refer to our entire device under active operation: that is, a single spin in a quantum dot subject to continuous charge detection by a QPC.

For applications in quantum information processing it is important to know the accuracy, or fidelity, of the single-shot spin read-out. The measurement fidelity is characterized by two parameters, α and β (inset to Fig. 4a), which we now determine for the data taken at 10 T.

The parameter α corresponds to the probability that the QPC current exceeds the threshold even though the electron was actually spin-↑, for instance due to thermally activated tunnelling or electrical noise (similar to 'dark counts' in a photon detector). The combined probability for such processes is given by the saturation value of the exponential fit in Fig. 3c, α, which depends on the value of the threshold current. We analyse the data in Fig. 3c using different thresholds, and plot α in Fig. 4b.

The parameter β corresponds to the probability that the QPC current stays below the threshold even though the electron was actually spin-↓ at the start of the read-out stage. Unlike α, β cannot be extracted directly from the exponential fit (note that the fit parameter $C = p(1 - \alpha - \beta)$ contains two unknowns: $p = \Gamma_\downarrow/(\Gamma_\uparrow + \Gamma_\downarrow)$ and β). We therefore estimate β by analysing the two processes that contribute to it. First, a spin-↓ electron can relax to spin-↑ before the electron tunnels out. This occurs with probability $\beta_1 = 1/(1 + T_1\Gamma_\downarrow)$. From a histogram (Fig. 4a) of the actual detection time, t_{detect} (Fig. 3b), we find $\Gamma_\downarrow^{-1} \approx 0.11$ ms, yielding $\beta_1 \approx 0.17$. Second, if the spin-↓ electron does tunnel off the dot but is replaced by a spin-↑ electron within about 8 μs, the resulting QPC step is too small to be detected. The probability that a step is missed, β_2, depends on the value of the threshold. It can be determined by applying a modified ('reversed') pulse (Fig. 3d). For such a pulse, we know that in each trace an electron is injected in the

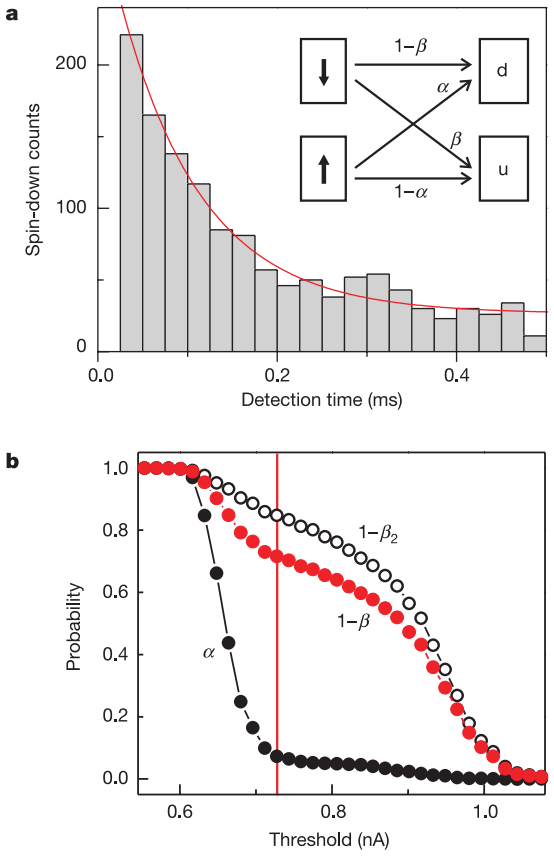

Figure 4 Measurement fidelity. **a**, Histogram showing the distribution of detection times, t_{detect}, in the read-out stage (see Fig. 3b for definition of t_{detect}). The exponential decay is due to spin-↓ electrons tunnelling out of the dot (rate = $\Gamma_\downarrow$) and due to spin flips during the read-out stage (rate = $1/T_1$). Red line: exponential fit with a decay time $(\Gamma_\downarrow + 1/T_1)^{-1}$ of 0.09 ms. Given that $T_1 = 0.55$ ms, this yields $\Gamma_\downarrow^{-1} \approx 0.11$ ms. Inset: fidelity parameters. A spin-↓ electron is declared 'down' (d) or 'up' (u) with probability $1 - \beta$ or β, respectively. A spin-↑ electron is declared 'up' or 'down' with probability $1 - \alpha$ or α, respectively. **b**, Closed black dots represent α, obtained from the saturation value of exponential fits as in Fig. 3c for different values of the read-out threshold. A current of 0.54 nA (0.91 nA) corresponds to the average value of ΔI_{QPC} when the dot is occupied (empty) during t_{read}. Open black dots: measured fraction of 'reverse-pulse' traces in which ΔI_{QPC} crosses the injection threshold (blue line in Fig. 3d). This fraction approximates $1 - \beta_2$, where β_2 is the probability of identifying a spin-↓ electron as 'spin-up' owing to the finite bandwidth of the measurement set-up. Closed red dots: total fidelity for the spin-↓ state, $1 - \beta$, calculated using $\beta_1 = 0.17$. The vertical red line indicates the threshold for which the visibility $1 - \alpha - \beta$ (separation between red and black closed dots) is maximal. This threshold value of 0.73 nA is used in the analysis of Fig. 3.

dot, so there should always be a step at the start of the pulse. The fraction of traces in which this step is nevertheless missed, that is, ΔI_{QPC} stays below the threshold (blue line in Fig. 3d), gives β_2. We plot $1-\beta_2$ in Fig. 4b (open dots). The resulting total fidelity for spin-↓ is given by $1-\beta \approx (1-\beta_1)(1-\beta_2)+(\alpha\beta_1)$. The last term accounts for the case when a spin-↓ electron is flipped to spin-↑, but there is nevertheless a step in ΔI_{QPC} due to the dark-count mechanism. In Fig. 4b we also plot the extracted value of $1-\beta$ as a function of the threshold.

We now choose the optimal value of the threshold as the one for which the visibility $1-\alpha-\beta$ is maximal (red line in Fig. 4b). For this setting, $\alpha \approx 0.07$, $\beta_1 \approx 0.17$ and $\beta_2 \approx 0.15$, so the measurement fidelity for the spin-↑ and the spin-↓ state is ~0.93 and ~0.72, respectively. The measurement visibility in a single-shot measurement is thus at present 65%.

Significant improvements in the spin measurement visibility can be made by lowering the electron temperature (smaller α), and especially by making the charge measurement faster (smaller β). Already, the demonstration of single-shot spin read-out and the observation of T_1 of the order of 1 ms are encouraging results for the use of electron spins as quantum bits. Present experiments focus on measuring the phase coherence time, T_2 (by definition $\leq 2T_1$), by performing pulsed electron spin resonance experiments. □

Received 6 April; accepted 25 May 2004; doi:10.1038/nature02693.

1. Sakurai, J. J. *Modern Quantum Mechanics* (Addison-Wesley, Reading, Massachusetts, 1994).
2. Wehrli, F. W. The origins and nature of nuclear magnetic resonance imaging. *Phys. Today* **6,** 34–42 (1992).
3. Wolf, S. A. *et al.* Spintronics: a spin-based electronics vision for the future. *Science* **294,** 1488–1495 (2001).
4. Blatt, R. & Zoller, P. Quantum jumps. *Eur. J. Phys.* **9,** 250–279 (1988).
5. Rugar, D., Budakian, R., Mamin, H. J. & Chui, B. W. Single spin detection by magnetic resonance force microscopy. *Nature* **430,** 329–332 (2004).
6. Loss, D. & DiVincenzo, D. P. Quantum computation with quantum dots. *Phys. Rev. A* **57,** 120–126 (1998).
7. Kane, B. E. A silicon-based nuclear spin quantum computer. *Nature* **393,** 133–137 (1998).
8. Vandersypen, L. M. K., *et al.* in *Quantum Computing and Quantum Bits in Mesoscopic Systems* (eds Legget, A. J., Ruggiero, B. & Silvestrini, P.) 201–209 (Kluwer Academic/Plenum, New York, 2003); ⟨http://xxx.lanl.gov/abs/quant-ph/0207059⟩ (2002).
9. Xiao, M., Martin, I. & Jiang, H. W. Probing the spin state of a single electron trap by random telegraph signal. *Phys. Rev. Lett.* **91,** 078301 (2003).
10. Friesen, M., Tahan, C., Joynt, R. & Eriksson, M. A. Spin readout and initialization in a semiconductor quantum dot. *Phys. Rev. Lett.* **92,** 037901 (2004).
11. Engel, H. *et al.* Measurement efficiency and n-shot read out of spin qubits. *Phys. Rev. Lett.* (in the press); preprint at ⟨http://xxx.lanl.gov/abs/cond-mat/0309023⟩ (2003).
12. Ionicioiu, R. & Popescu, A. E. Single spin measurement using spin-orbital entanglement. Preprint at ⟨http://xxx.lanl.gov/abs/quant-ph/0310047⟩ (2003).
13. Greentree, A. D., Hamilton, A. R., Hollenberg, L. C. L. & Clark, R. G. Electrical readout of a spin qubit without double occupancy. Preprint at ⟨http://xxx.lanl.gov/abs/cond-mat/0403449⟩ (2004).
14. Kouwenhoven, L. P., Austing, D. G. & Tarucha, S. Few-electron quantum dots. *Rep. Prog. Phys.* **64,** 701–736 (2001).
15. Weis, J., Haug, R. J., von Klitzing, K. & Ploog, K. Lateral transport through a single quantum dot with a magnetic field parallel to the current. *Surf. Sci.* **305,** 664–668 (1994).
16. Kouwenhoven, L. P. *et al.* Excitation spectra of circular, few-electron quantum dots. *Science* **278,** 1788–1792 (1997).
17. Ciorga, M. *et al.* Readout of a single electron spin based quantum bit by current detection. *Physica E* **11,** 35–40 (2001).
18. Fujisawa, T., Austing, D. G., Tokura, Y., Hirayama, Y. & Tarucha, S. Allowed and forbidden transitions in artificial hydrogen and helium atoms. *Nature* **419,** 278–281 (2002).
19. Hanson, R. *et al.* Zeeman energy and spin relaxation in a one-electron quantum dot. *Phys. Rev. Lett.* **91,** 196802 (2003).
20. Folk, J. A., Potok, R. M., Marcus, C. M. & Umansky, V. A gate-controlled bidirectional spin filter using quantum coherence. *Science* **299,** 679–682 (2003).
21. Lu, W., Ji, Z., Pfeiffer, L., West, K. W. & Rimberg, A. J. Real-time detection of electron tunnelling in a quantum dot. *Nature* **423,** 422–425 (2003).
22. Fujisawa, T., Hayashi, T., Hirayama, Y., Cheong, H. D. & Jeong, Y. H. Electron counting of single-electron tunnelling current. *Appl. Phys. Lett.* **84,** 2343–2345 (2004).
23. Elzerman, J. M. *et al.* Few-electron quantum dot circuit with integrated charge read out. *Phys. Rev. B* **67,** 161308 (2003).
24. Elzerman, J. M., Hanson, R., Willems van Beveren, L. H., Vandersypen, L. M. K. & Kouwenhoven, L. P. Excited-state spectroscopy on a nearly-closed quantum dot via charge detection. *Appl. Phys. Lett.* **84,** 4617–4619 (2004).
25. Field, M. *et al.* Measurements of Coulomb blockade with a noninvasive voltage probe. *Phys. Rev. Lett.* **70,** 1311–1314 (1993).
26. Hanson, R. *et al.* Semiconductor few-electron quantum dot operated as a bipolar spin filter. Preprint at ⟨http://xxx.lanl.gov/abs/cond-mat/0311414⟩ (2003).
27. Khaetskii, A. V. & Nazarov, Y. V. Spin-flip transitions between Zeeman sublevels in semiconductor quantum dots. *Phys. Rev. B* **64,** 125316 (2001).
28. Golovach, V. N., Khaetskii, A. & Loss, D. Phonon-induced decay of the electron spin in quantum dots. Preprint at ⟨http://xxx.lanl.gov/abs/cond-mat/0310655⟩ (2003).
29. Woods, L. M., Reinecke, T. L. & Lyanda-Geller, Y. Spin relaxation in quantum dots. *Phys. Rev. B* **66,** 161318 (2002).
30. Erlingsson, S. I. & Nazarov, Y. V. Hyperfine-mediated transitions between a Zeeman split doublet in GaAs quantum dots: The role of the internal field. *Phys. Rev. B* **66,** 155327 (2002).

Supplementary Information accompanies the paper on **www.nature.com/nature**.

Acknowledgements We thank D. P. DiVincenzo, H. A. Engel, T. Fujisawa, V. Golovach, Y. Hirayama, D. Loss, T. Saku, R. Schouten and S. Tarucha for technical support and discussions. This work was supported by the DARPA-QUIST programme, the ONR, the EU-RTN network on spintronics and the Dutch Organisation for Fundamental Research on Matter (FOM).

Competing interests statement The authors declare that they have no competing financial interests.

Correspondence and requests for materials should be addressed to L.M.K.V. (lieven@qt.tn.tudelft.nl).

Electrical detection of the spin resonance of a single electron in a silicon field-effect transistor

M. Xiao[1], I. Martin[2], E. Yablonovitch[3] & H. W. Jiang[1]

[1]*Department of Physics and Astronomy, University of California, Los Angeles, California 90095, USA*
[2]*Theoretical Division, Los Alamos National Laboratory, Los Alamos, New Mexico 87545, USA*
[3]*Department of Electrical Engineering, University of California, Los Angeles, California 90095-1594, USA*

The ability to manipulate and monitor a single-electron spin using electron spin resonance is a long-sought goal. Such control would be invaluable for nanoscopic spin electronics, quantum information processing using individual electron spin qubits and magnetic resonance imaging of single molecules. There have been several examples[1,2] of magnetic resonance detection of a single-electron spin in solids. Spin resonance of a nitrogen-vacancy defect centre in diamond has been detected optically[3], and spin precession of a localized electron spin on a surface was detected[4,5] using scanning tunnelling microscopy. Spins in semiconductors are particularly attractive for study because of their very long decoherence times[6]. Here we demonstrate electrical sensing of the magnetic resonance spin-flips of a single electron paramagnetic spin centre, formed by a defect in the gate oxide of a standard silicon transistor. The spin orientation is converted to electric charge, which we measure as a change in the source/drain channel current. Our set-up may facilitate the direct study of the physics of spin decoherence, and has the practical advantage of being composed of test transistors in a conventional, commercial, silicon integrated circuit. It is well known from the rich literature of magnetic resonance studies that there sometimes exist structural paramagnetic defects[7] near the Si/SiO_2 interface. For a small transistor, there might be only one isolated trap state that is within a tunnelling distance of the channel, and that has a charging energy close to the Fermi level.

When a defect is present, the source/drain channel current can experience random telegraph signal (RTS), jumping between two discrete current values. These arise from two possible trapped electric charge states of the defect. The two charge states can correspond to the two spin orientations of a trapped electron. Field effect transistor (FET) current senses electrostatic charge (by definition), and can thus sense single-electron spin resonance.